Spine-like Joint Link Mechanism to Design Wearable Assistive Devices with Comfort and Support

Jungyeong Kim[1,3], Jungsan Cho[2,3], Jinhyeon Kim[3]
Jin Tak Kim[3], Sangchul Han[3], Sangshin Park[3] and Han Ul Yoon[4]

***Abstract*— When we develop wearable assistive devices comfort and support are two main issues needed to be considered. In conventional design approaches, the degree of freedom of wearer's joint movement tends to be oversimplified. Accordingly, the wearer's motion becomes restrained and bone/ligament injuries might occur in case of unexpected fall. To mitigate those issues, this letter proposes a novel joint link mechanism inspired by a human spine structure as well as functionalities. The key feature of the proposed spine-like joint link mechanism is that hemispherical blocks are concatenated via flexible synthetic fiber lines so that their concatenation stiffness can be adjusted according to a tensile force. This feature has a great potentiality for designing a wearable assistive devices that can support aged people's sit-to-stand action or augment a spinal motion by regulating the concatenation stiffness. In addition, the concatenated hemispherical blocks enables the wearer to move his/her joint with the full degree of freedom, which in turn, increases wearer's mobility and prevents joint misalignment. The experimental results with a testbed and a pilot wearer substantiated that the spine-like joint link mechanism can serve as a key component to design the wearable assistive devices for better mobility and safety.**

I. Introduction

Wearable assistive robots have been used for various applications, e.g., quiet balance support for elderly people [1]–[3], gait function rehabilitation for stroke survivors [4]–[6], heavy object lifting for manual workers [7]–[9], mobility augmentation for soldiers in challenging battle fields [10]–[12], and so on. Since the wearable assistive robots have shown great potential in a broad range of applications, many studies are now underway to extend their usage as human assistive devices.

At the early stage of wearable assistive robots, design approaches tended to simplify human joint-link mechanism. For example, a knee joint was typically simplified as a hinge type joint with a single degree of freedom (DoF), which in turn restricted thigh and shin movement only into a sagittal plane [13]–[16]. Moreover, most of the wearable assistive robots have been made by rigid materials although they targeted to support various body parts such as lower-limb [13]–[20], lower-back [21], [22], upper-limb [23], [24], and hand [25], [26]. The rigidity of the wearable assistive robots might facilitate "enough support" in sense of force/torque generation; whereas, the length of a link could not be changed. Consequently, in addition to the aforesaid sagittal plane restriction, wearer's joint-link movement was constrained by a loss of flexibility in length.

The wearer's constrained joint-link movement are well-exemplified by existing early-designed exoskeletons. Low-limb exoskeletons such as EXPOS [13], BLEEX [14], HAL [15], eLEGS [16] commonly employed a uniaxial revolute joint model for a wearer's knee joint, which was simplified to 1-DoF model. Studies in [18]–[21] presented exoskeletons to support wearer's lower-back as well as lower-limb. The presented exoskeletons could retain the wearer's lower-back to be upright position by supporting a lumber spine with a rigid structure, and the wearer's knee joint was simplified as a hinge type joint. Under all constrained design approaches above, kinematic discrepancy between the wearer's joint and the exoskeleton's joint movements becomes inevitable.

The kinematic discrepancy between a human wearer and an exoskeleton robot indeed causes somewhat problematic issues. Even though the ranges of motion of hip/knee/ankle joints are rather limited, they are able to move toward medial-lateral direction as well as anterior-posterior direction. Namely, the hip/knee/ankle joints are not perfect spherical joints, but their movements are still closer to that of the spherical joints [27], [28]. Therefore, the kinematic discrepancy can cause unnatural walking and discomfort to the wearer while performing daily activities. Moreover, the reduced DoF due to the simplified kinematics makes the wearer exposed to serious joint or ligament injuries when the wearer tries bending/leaning toward medial-lateral direction [28].

Wearable robots made by soft materials have been thought as a feasible solution to alleviate both kinematic discrepancy and joint misalignment problem. Accordingly, various soft-type wearable robots have been developed, e.g., exo-suit [10], exo-glove [29], soft power suit [30], inflatable soft wearable robot [31], [32], and so on. Compared to the rigid-type wearable robots, the soft-type ones less constrains natural joint movement, which in turn reduces discomfort caused by joint misalignment. The limitation of the soft-

*This work was partially supported by the Korea Institute of Industrial Technology under "Development of Soft Robotics Technology for Human-Robot Coexistence Care Robots (KITECH EH210010)" and by the Ministry of Trade, Industry & Energy (MOTIE, Korea) under "the Industrial Strategic Technology Development Program (20007836, Development of Wearable robot for Construction Workers)"

[1] Robotics and Virtual Engineering, University of Science and Technology (UST), Daejon, 34113, South Korea. Email: kjy880527@kitech.re.kr

[2] Robotics and Industrial Technology, University of Science and Technology (UST), Daejon, 34113, South Korea. Email: chojs@kitech.re.kr

[3] Applied Robot R&D Department, Korea Institute of Industrial Technology (KITECH), Ansan, 15588, South Korea. Email: {qkrb0117, jintagi, pss, bomber21}@kitech.re.kr

[4] Division of Software, Yonsei University, Wonju, 26493, South Korea. Email: huyoon@yonsei.ac.kr

type wearable robots is, however, that they generate less assistive force/torque than that of the rigid-type. For instance, the soft-type wearable robots allows force/torque which is originally generated by wearer's muscle to be increased by 10 percent through 100 percent (which means doubled); in contrast, the rigid-type ones does 100 percent through 1000 percent (which represents 10 times increment) [33]. Due to this limitation, the soft-type ones have been narrowly applied for, e.g., wrist support, forearm assistance, ankle support, etc.

To mitigate above-mentioned issues of rigid/soft-type wearable robots, this letter proposes a novel joint link mechanism which was inspired by the dexterous characteristics of a human spine. Specifically speaking, the distinguished feature of the proposed mechanism is that multiple hemispherical blocks are concatenated through synthetic fiber lines and rubber strips to functionally mimic the vertebrae, tendon, and ligament of the spine; accordingly, it will be referred to as a spine-like joint link mechanism (SJLM) throughout this letter. The design of the SJLM mainly aimed at bestowing a capability of adjusting its stiffness/flexibility to assist a wearer with comfort and support. This capability enables the SJLM to be utilized as a key component to develop wearable robots with the following advantages:

1) *Under high-stiffness (low-flexibility) adjustment, the SJLM can support the wearer with desired assistive force*: This advantage is well-exemplified by the existing Chair Exoskeleton (CEX) of Hyundai Motor Group [34] (see Fig. 1(a)).
2) *Under low-stiffness (high-flexibility) adjustment, the SJLM can provide the wearer with comfort by alleviating kinematic discrepancy and joint misalignment*: As presented in [35], for instance, HeroWear Apex suit – a biomechanically-assistive garment to support a lumber spine – are comfort to wear as well as lightweighted (see Fig. 1(b)).

This letter is organized as follows. In Sec. 2, the design of the SJLM is presented. Specifically, components design, fabrication, dexterous functionalities are explained. Section 3 discusses an input-out relationship of the SJLM, which corresponds to a tensile force under a hydraulic actuation versus an assistive force generated at an end-link part.

(a) (b)

Fig. 1. (a) Chair Exoskeleton (CEX) developed by Huyndai Motor Group [34], (b) HeroWear Apex suit developed by HeroWear LLC [35].

Section 4 presents the experimental procedures and results to substantiate the input-output relationship and the maximum supporting capabilities. Two feasible SJLM applications are introduced as well. Section 5 will be the conclusion of this letter.

II. Design of Spine-like Joint Link Mechanism

A. Structure Overview

Figure 2 illustrates a SJLM design inspired by a human spine and functional correspondences and presents the fabricated SJLM. Figure 2(a) shows bones, muscles and tendons, ligaments, and cartilages which are also referred to as vertebral body, erector spinae, anterior/posterior longitudinal ligaments, and intervertebral discs in terms of anatomic jargon, respectively. Inspired by this anatomical structure and functionalities, as presented in Fig. 2(b), the SJLM was designed with hemispherical blocks, hydraulic actuator, synthetic fiber lines, silicon-based strip, and natural rubber discs which functionally correspond to bones, muscles and tendons, ligaments, and cartilages, respectively. Figure 2(c) shows the fabricated SJLM.

B. Components Design and Fabrication

Recall that the components of the SJLM and their functional correspondences were presented in Fig. 2(b); namely, hemispherical block (bone), hydraulic actuator and synthetic fiber lines (muscles and tendons), silicon-based strips (ligaments), and natural rubber discs (cartilages). In order to mimic a human spine movement characteristics as well as anatomy, the SJLM was assembled by concatenating the hemispherical blocks (3D printed with ABS filament) via the four synthetic fiber lines (Dyneema Liros D-Pro SK78/2mm/red/410kgf breaking strength, Liros, GmbH). Studies in [27], [36]–[38] proposed the mechanical design-based approaches to constrain the wearer's movement within a safe range. In contrast, the silicon-based strips were employed as flexible constraints for our SJLM to guarantee redundant configurations as well as the wearer's full DoF

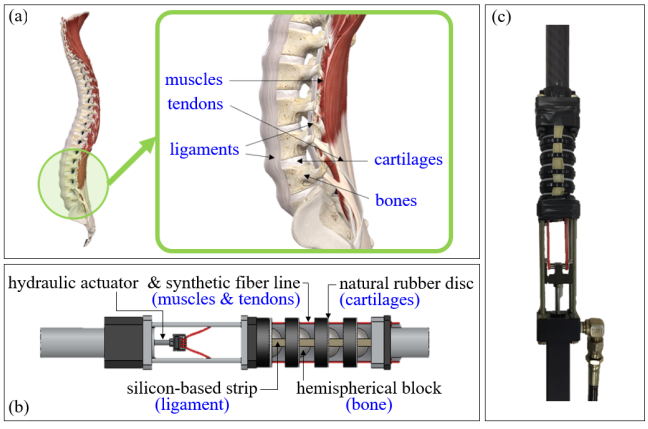

Fig. 2. The SJLM design inspired by a human spine and functional correspondences: (a) human spine anatomy (excerpted and redrawn from https://3d4medical.com), (b) SJLM components, (c) the fabricated SJLM.

movement. The natural rubber discs were inserted between the hemisphere blocks to serve as damper/suspension against impulsive external forces.

C. Dexterous Functionalities with Adjustable Stiffness

Figure 3 shows the stiffness adjustment mechanism of the SJLM according to hydraulic actuation. We note that SJLM part is presented by a cross-sectional view with only two synthetic fiber lines (top and bottom) to explicitly illustrate the configuration of the SJLM when the lines are pulled/released. Recall that all hemispherical blocks and the end-link part are indeed concatenated via four synthetic fiber lines. As depicted in Fig. 3(a), when the lines are totally loosened by a hydraulic actuation, the concatenation of all hemispherical blocks are detached. Accordingly, both hemispherical blocks and the end-link part can move freely and the SJLM has the minimum stiffness. Figure 3(b) presents when the lines are fully tightened; accordingly, the hemispherical blocks and the end-link part are aligned straightly. The SJLM has the maximum stiffness under this configuration. If the line tightness is set to in-between, then the SJLM can play a role of an elastic link component. In sum, the configuration as well as the stiffness of the SJLM is adjustable under our design mechanism by varying the tensile force of the synthetic fiber lines.

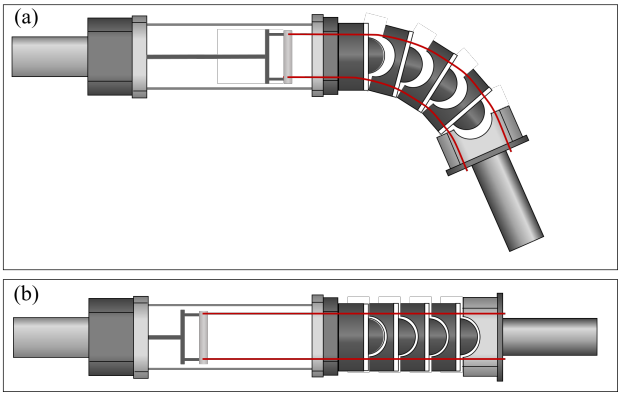

Fig. 3. The stiffness adjustment mechanism of the SJLM according to hydraulic actuation: (a) when the the tension of synthetic fiber lines is fully loosened and b) when the tension of synthetic fiber lines is fully tightened.

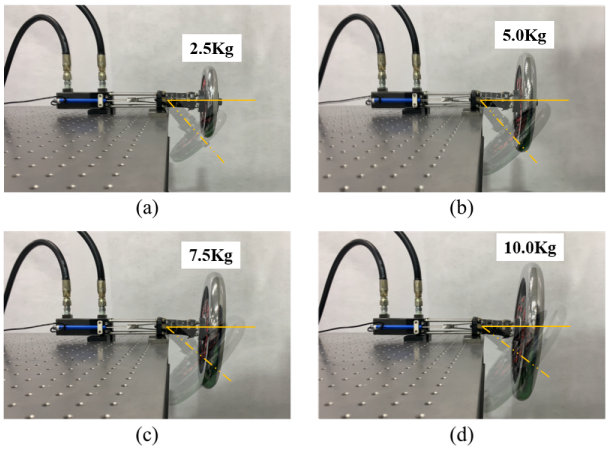

Fig. 4. The weight lifting and supporting capability of the SJLM (the transparent represent initial positions and the opaque are final positions): (a) 2.5kg weight, (b) 5kg weight, (c) 7.5kg weight, (d) 10kg weight.

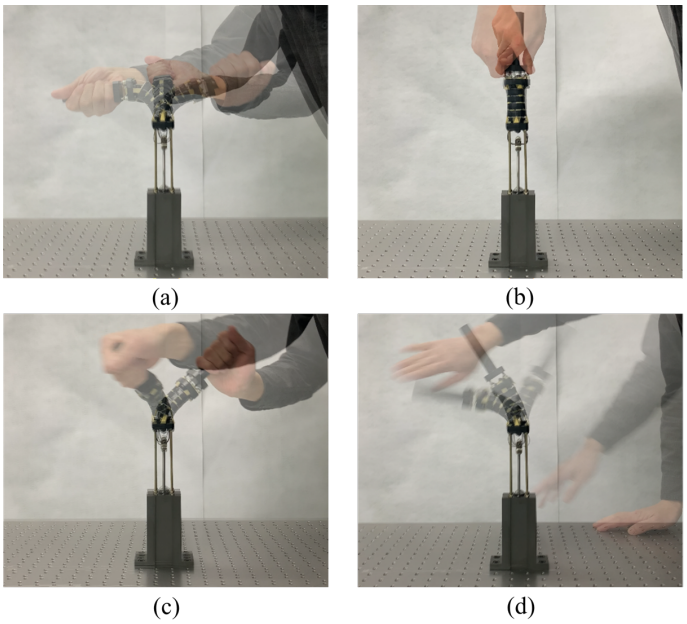

Fig. 5. The demonstration of dexterous functionalities of the SJLM: (a) flexion and extension up to ± 90 degrees, (b) axial torsion, (c) flexible manipulatability in 3D, and (d) restoration after applying an external force,

The above-mentioned adjustable stiffness bestows the SJLM with dexterous functionalities. Figure 4 shows the weight lifting and supporting capability of the SJLM. As shown in Fig. 4(a) through 4(d), the SJLM can lift up various weights ranging from 2.5kg to 10kg, then sustain its configuration while supporting the weight. Figure 5 demonstrates that the SJLM can play a role of an elastic link. Figure 5(a) through 5(d) show that flexion and extension up to ± 90 degrees, axial torsion, flexible manipulatability in 3D, and restoration after applying an external force, respectively. All these demonstrated functionalities substantiate that the SJLM can be utilized to design wearable assistive systems. For instance, suppose that the two links of SJLM are attached to the thigh and the shin of a wearer so that its hemispherical blocks are aligned with a knee joint. By gradually tightening/loosening the line tension, the SJLM can support the wearer to perform sit-to-stand (and vice versa, stand-to-sit action) safely. Also, serious knee injuries, e.g., twist or sprain, can be prevented since the SJLM preserves the full DoF of the wearer's knee movement.

III. Modeling an Input-Output Relationship of Spline-like Joint Link Mechanism

A relationship between a tensile force on four synthetic fiber lines under hydraulic actuation and an assistive force generated by an end-link can be modeled as input-output relationship. Te derive the input-output relationship model, we employ a simplified free body diagram in which a

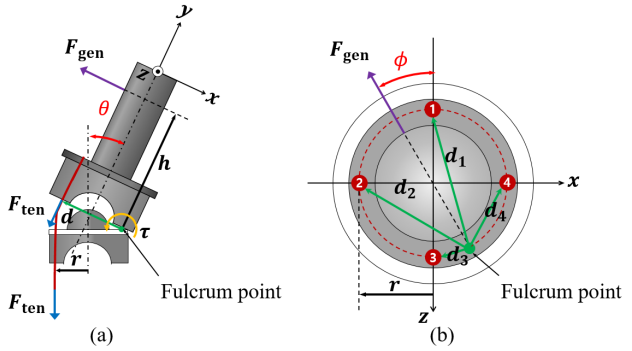

Fig. 6. Employed lever system model to analyze an input-output relationship between $\boldsymbol{F}_{\text{ten}}$ and $\boldsymbol{F}_{\text{gen}}$: (a) the side view ($x$-$y$ plane) of the last hemispherical block and the link and (b) the top view (x-z plane) of the last hemispherical block.

hemispherical block and the end-link works as a line-attached lever system with a fulcrum as illustrated in Figure 6. The effect of friction between the hemisphere blocks and the synthetic fiber lines will be concerned at the last part of this derivation.

From Fig. 6(a), $\boldsymbol{F}_{\text{ten}}$ and $\boldsymbol{F}_{\text{gen}}$ denote the tensile force induced by tightening the synthetic fiber lines under hydraulic actuation and the generated force by the end-link, respectively. Since the end-link is of cylinderical shape, we can assume that the direction of $\boldsymbol{F}_{\text{gen}}$ is passing through the center of the end-link and acting toward a radial direction. $\boldsymbol{r}$ is a vector from the center of the hemispherical block to the center of a line. A vector $\boldsymbol{h}$ points from the fulcrum point to the point on where $\boldsymbol{F}_{\text{gen}}$ is generated. We note that, from now on, a boldface symbol represents a vector and a nonboldface symbol does its length, i.e., $\|\boldsymbol{r}\| = r$.

From Fig. 6(b), let $\boldsymbol{d}_1, \boldsymbol{d}_2, \boldsymbol{d}_3$ and $\boldsymbol{d}_4$ denote vectors from the fulcrum point to the center of each line, respectively. Suppose that the four lines are tightened by $\boldsymbol{F}_{\text{ten}}$, then a total torque $\boldsymbol{\tau}$ produced at the fulcrum point is

$$\boldsymbol{\tau} = \boldsymbol{d}_1 \times \boldsymbol{F}_{\text{ten}} + \boldsymbol{d}_2 \times \boldsymbol{F}_{\text{ten}} + \boldsymbol{d}_3 \times \boldsymbol{F}_{\text{ten}} + \boldsymbol{d}_4 \times \boldsymbol{F}_{\text{ten}} \quad (1)$$

where,

$$\begin{aligned} d_1 &= \sqrt{2r^2 - 2r^2\cos(\pi - \phi)}, \\ d_2 &= \sqrt{2r^2 - 2r^2\cos(\frac{\pi}{2} + \phi)}, \\ d_3 &= \sqrt{(2r)^2 - (d_1)^2}, \\ d_4 &= \sqrt{(2r)^2 - (d_2)^2}. \end{aligned} \quad (2)$$

which can be easily identified from geometric relationships depicted in From Fig. 6(b). The torque $\boldsymbol{\tau}$ can also be expressed in terms of $\boldsymbol{h}$ and $\boldsymbol{F}_{\text{ten}}$ as

$$\boldsymbol{\tau} = \boldsymbol{h} \times \boldsymbol{F}_{\text{gen}} \quad (3)$$

From Eq. (1) and Eq. (3), the relationship between $\boldsymbol{F}_{\text{ten}}$ and $\boldsymbol{F}_{\text{gen}}$ is

$$(\boldsymbol{d}_1 + \boldsymbol{d}_2 + \boldsymbol{d}_3 + \boldsymbol{d}_4) \times \boldsymbol{F}_{\text{ten}} = \boldsymbol{h} \times \boldsymbol{F}_{\text{gen}}. \quad (4)$$

Due to the symmetric placement of the SJLM fiber lines, $\boldsymbol{d}_1 + \boldsymbol{d}_2 + \boldsymbol{d}_3 + \boldsymbol{d}_4$ yields a vector of which length is always equal to $4r$ and direction is aligned with $\boldsymbol{F}_{\text{gen}}$ as ϕ in x-z plane. Therefore, from Eq. (4), we can obtain the input-output relationship between the amount of the tensile force, F_{ten} (input), and the amount of the generated force, F_{gen} (output), as

$$F_{\text{gen}} = \frac{4r}{h} F_{\text{ten}} \quad (5)$$

which implies that F_{gen} linearly increases. Also, for all ϕ and θ, the same amount of force is generated. Lastly, we consider a friction between the four lines and hemispherical blocks as a nonlinear friction term, denoted by $\varphi(F_{\text{ten}}, \theta, \phi)$, which might be expected to show a hysteresis (since the motion of the four lines passing though hemisphere block is conceptually similar to a tunneling behavior). Hence, from Eq. (5), we obtain the input-output relationship

$$F_{\text{gen}} = \frac{4r}{h} F_{\text{ten}} - \varphi(F_{\text{ten}}, \theta, \phi) \quad (6)$$

Note that, this theoretically obtained linear relationship between F_{ten} and F_{gen} will be substantiated in the following section.

IV. Experiments and Results

The following three experiments were performed to substantiate the derived input-output relationship between F_{ten} and F_{gen} (Sec. IV-A), identify the maximum supporting capabilities under the maximum tensile force setup which can serve as a technical specification (Sec. IV-B), and test the feasibility to be utilized as a key component for the design of wearable assistive devices (Sec. IV-C). Discussions about the results will be followed right after each experiment.

A. Substantiating the input-output relationship of the SJLM

Figure 7 shows the experimental setup to substantiate the derived input-output relationship (namely, a tensile force F_{ten} versus a generated force F_{gen} relationship) which was presented in Eq. (6). A desired value of F_{ten} could be set by using a pressure sensor (LM-PPT-H, Lumax Aerospace Corp.). Meanwhile, F_{gen} was measured by a push-pull gauge (FGP-50, 0.01kgf resolution, maximum measured force 50kgf, Nidec-Shimpo Co.).

The experiment was performed by the following procedures:

1) Install a testbed with setting the SJLM at a specific angle, e.g., $\theta = 80°$.
2) Increase F_{ten} gradually by a hydraulic actuation and measure F_{ten} and F_{gen}.
3) Repeat the above procedures for $\theta = 50°$, $\theta = 20°$, in sequel.

Under our design, r and h were set to 11mm and 90mm, respectively. Figure 7(b) through 7(d) present the testbed installment for $\theta = 80°$, $\theta = 50°$, and $\theta = 20°$, respectively. The radial direction ϕ was set to $45°$ for all conditions.

Figure 8 presents the substantiated input-output (a tensile force F_{ten} versus a generated force F_{gen}) relationship of the

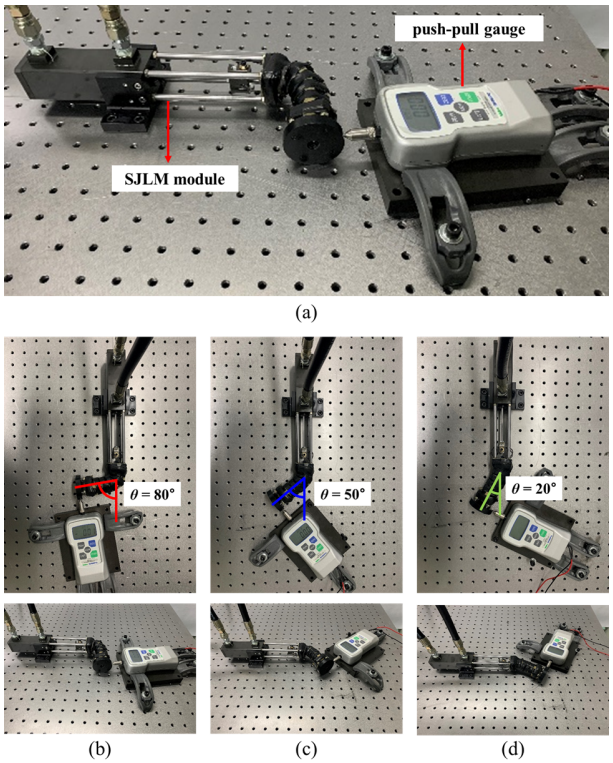

Fig. 7. The experimental setup to substantiate the input(F_{ten})-output(F_{gen}) relationship: (a) a testbed consists of the SJLM module and a push-pull gauge. (b), (c) and (d) are experimental setups for $\theta = 80°$, $\theta = 50°$, $\theta = 20°$, respectively. ϕ was set to $45°$ for all conditions.

SJLM. By recalling Eq. (6) and substituting $r = 11$ and $h = 90$, we have

$$\begin{aligned} F_{\text{gen}} &= \frac{4 \cdot 11}{90} F_{\text{ten}} - \varphi(F_{\text{ten}}, \theta, \phi) \\ &= 0.489 F_{\text{ten}} - \varphi(F_{\text{ten}}, \theta, \phi). \end{aligned} \tag{7}$$

From Fig. 8, the slope of F_{ten} versus F_{gen} curve are approximately

$$\begin{aligned} \frac{F_{\text{gen}}}{F_{\text{ten}}} &\simeq \frac{120}{300} = 0.400 \quad \text{when} \quad \theta = 80° \\ \frac{F_{\text{gen}}}{F_{\text{ten}}} &\simeq \frac{110}{300} \simeq 0.367 \quad \text{when} \quad \theta = 50° \\ \frac{F_{\text{gen}}}{F_{\text{ten}}} &\simeq \frac{100}{300} \simeq 0.333 \quad \text{when} \quad \theta = 20° \end{aligned}$$

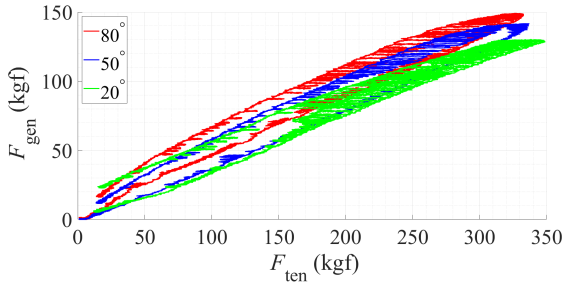

Fig. 8. The substantiated input-output (a tensile force F_{ten} versus a generated force F_{gen}) relationship of the SJLM.

which allows us to presumably estimate the effect of a frictional force $\varphi(F_{\text{ten}}, \theta, \phi)$ from Eq. (7) as follows:

$$\begin{aligned} \varphi(F_{\text{ten}}, 80°, 45°) &\simeq 0.089 F_{\text{ten}} \quad \text{when} \quad \theta = 80° \\ \varphi(F_{\text{ten}}, 50°, 45°) &\simeq 0.122 F_{\text{ten}} \quad \text{when} \quad \theta = 50° \\ \varphi(F_{\text{ten}}, 20°, 45°) &\simeq 0.156 F_{\text{ten}} \quad \text{when} \quad \theta = 20° \end{aligned}$$

However, since F_{ten} versus F_{gen} curve shows an obvious nonlinear hysteresis, $\varphi(F_{\text{ten}}, \theta, \phi)$ needs to be identified further. Compared to our result, the similar hysteresis plots has been introduced in [39] as well. The nonlinear hysteresis would be precisely approximated by adopting a neural net-based approaches.

Suppose that $h = 157$mm which is a half of shank length as presented in [40]. We then calculate the maximum assistive torque from Eq. (3)

$$\begin{aligned} \tau &= h F_{\text{gen}} \\ &= 0.157[\text{m}] \times 0.4889 \times 378[\text{kgf}] \times 9.81[\text{m/s}^2] \\ &= 284.63[\text{Nm}] \simeq 285[\text{Nm}] \end{aligned} \tag{8}$$

This value is competitive to the existing lower-limb exoskeletons such as presented in [14], [18], [21] of which the maximum assistance force ranging from 50.0Nm to 200.0Nm.

B. The maximum supporting capabilities of the SJLM under the maximum tensile force

Figure 9 shows the experimental setup to measure the maximum supporting capabilities of the SJLM under the maximum tensile force, which can serve as a technical specification of the SJLM. An absolute digimatic indicator (ID-S112XB, 0.001mm resolution, Mitutoyo Co.) and a push-pull gauge (FGP-50, 0.01kgf resolution, maximum measured force 50kgf, Nidec-Shimpo Co.) were used to measure an applied force and a corresponding displacement, respectively. The goal of this experiment was to identify the maximum supporting capabilities of the SJLM in terms of the maximum translation and rotational stiffness. The experiment was performed as follows:

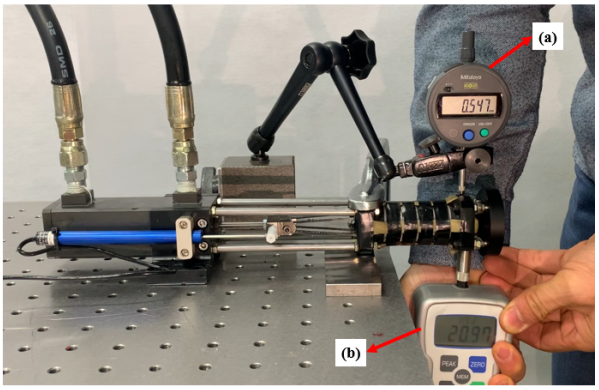

Fig. 9. The experimental setup to measure various SJLM properties under the maximum tensile force: (a) an absolute digimatic indicator to measure a displacement and (b) a push-pull gauge to measure a force applied to the SJLM.

1) Apply the maximum tensile force F_{ten} to the SJLM.
2) Push the SJLM upward by the push-pull gauge and measure a force applied to the SJLM.
3) Meanwhile, measure the displacement of the SJLM by the absolute digimatic indicator.

From the experiment, the measured translational displacement was 0.547mm which corresponded to the rotational displacement 6.15x10^{-2}rad according to a torque arm 89mm when the applied force was 20.97kgf (205.7N); in terms of torque 18.3Nm. This results indicated that, under the maximum tensile force setting, the maximum translational and rotational stiffness of the SJLM were 376.1kN/m and 2.98×10^{3}Nm/rad, respectively. These resulting values are competitive to the joint stiffness of Dexter arm [41], [42] consisting of gearbox, motor and steel wire, which is prevalently used for exoskeletons [13], [22]–[26].

C. Feasible SJLM applications: wearable lower-limb and spine assistive devices

Figure 10 shows the two feasible applications of the SJLM. First, a wearable low-limb assistive device is presented in Fig. 10(a). Two SJLMs are mounted on the lateral sides of pilot wearer's legs; specifically, the hemisphere block parts are aligned with the wearer's knee joints. If the SJLM were set to high stiffness adjustment, then the pilot wearer could maintain the upright position for longer time but spend less musculo-skeletal power. Figure 10(b) demonstrates that the SJLM can be bent with elasticity while the DoF for the wearer's movement being preserved. Nest, Fig. 10(c) presents a spine assistive device designed as a harness type. From Fig. 10(d), we can see that the pilot wearer's spine (especially a lumber-thoracic spine) can be supported by the SJLM. This type of wearable assistive device will be helpful for workers who need to sustain upright posture for a long time, e.g., mart cashiers, security guards, and so on.

Fig. 10. The two SJLM applications: (a) a lower-limb assistive device under high stiffness adjustment and (b) it can be bent with elasticity under low stiffness adjustment, (c) and (d) a spine assistive device designed as a harness type to support a lumber-thoracic spine.

V. Conclusions

This letter proposed a spine-like joint link mechanism (SJLM) for designing wearable assistive devices with comport and support, which guarantees better mobility and safety. Inspired by a human spine structure, the SJLM was made of the concatenation of multiple hemispherical blocks via four synthetic fiber lines. The concatenation stiffness of the hemispherical blocks could be adjusted by regulating the tensile force on the lines under a hydraulic actuation, which in turn, generated a supporting force at the end-link of the SJLM. The experimental results substantiated the feasibility of the SJLM to be utilized as a key component for designing wearable assistive devices by identifying an input-output characteristics as well as the maximum supporting capabilities under the maximum tensile force setup. Two SJLM applications were presented to demonstrate the substantiated feasibility, which were wearable low-limb and spine assistive devices. This study will be culminated to the design of the innovated version of wearable assistive devices such as a lower-limb exoskeleton or an upper-limb augmentation device as future works.

References

[1] D. Martelli, F. Vannetti, M. Cortese, P. Tropea, F. Giovacchini, S. Micera, V. Monaco, and N. Vitiello, "The effects on biomechanics of walking and balance recovery in a novel pelvis exoskeleton during zero-torque control," *Robotica*, vol. 32, no. 8, pp. 1317–1330, 2014.

[2] V. Monaco, P. Tropea, F. Aprigliano, D. Martelli, A. Parri, M. Cortese, R. Molino-Lova, N. Vitiello, and S. Micera, "An ecologically-controlled exoskeleton can improve balance recovery after slippage," *Scientific reports*, vol. 7, no. 1, pp. 1–10, 2017.

[3] I. Farkhatdinov, J. Ebert, G. Van Oort, M. Vlutters, E. Van Asseldonk, and E. Burdet, "Assisting human balance in standing with a robotic exoskeleton," *IEEE Robotics and automation letters*, vol. 4, no. 2, pp. 414–421, 2019.

[4] D. R. Louie and J. J. Eng, "Powered robotic exoskeletons in post-stroke rehabilitation of gait: a scoping review," *Journal of neuroengineering and rehabilitation*, vol. 13, no. 1, pp. 1–10, 2016.

[5] M. Bortole, A. Venkatakrishnan, F. Zhu, J. C. Moreno, G. E. Francisco, J. L. Pons, and J. L. Contreras-Vidal, "The h2 robotic exoskeleton for gait rehabilitation after stroke: early findings from a clinical study," *Journal of neuroengineering and rehabilitation*, vol. 12, no. 1, pp. 1–14, 2015.

[6] J. F. Veneman, R. Kruidhof, E. E. Hekman, R. Ekkelenkamp, E. H. Van Asseldonk, and H. Van Der Kooij, "Design and evaluation of the lopes exoskeleton robot for interactive gait rehabilitation," *IEEE Transactions on Neural Systems and Rehabilitation Engineering*, vol. 15, no. 3, pp. 379–386, 2007.

[7] S. Alabdulkarim, S. Kim, and M. A. Nussbaum, "Effects of exoskeleton design and precision requirements on physical demands and quality in a simulated overhead drilling task," *Applied ergonomics*, vol. 80, pp. 136–145, 2019.

[8] S. Kim, M. A. Nussbaum, M. I. M. Esfahani, M. M. Alemi, S. Alabdulkarim, and E. Rashedi, "Assessing the influence of a passive, upper extremity exoskeletal vest for tasks requiring arm elevation: Part i–"expected" effects on discomfort, shoulder muscle activity, and work task performance," *Applied ergonomics*, vol. 70, pp. 315–322, 2018.

[9] M. Fontana, R. Vertechy, S. Marcheschi, F. Salsedo, and M. Bergamasco, "The body extender: A full-body exoskeleton for the transport and handling of heavy loads," *IEEE Robotics & Automation Magazine*, vol. 21, no. 4, pp. 34–44, 2014.

[10] A. T. Asbeck, S. M. De Rossi, K. G. Holt, and C. J. Walsh, "A biologically inspired soft exosuit for walking assistance," *The International Journal of Robotics Research*, vol. 34, no. 6, pp. 744–762, 2015.

[11] R. Gopura, D. Bandara, K. Kiguchi, and G. K. Mann, "Developments in hardware systems of active upper-limb exoskeleton robots: A review," *Robotics and Autonomous Systems*, vol. 75, pp. 203–220, 2016.

[12] K. N. Gregorczyk, L. Hasselquist, J. M. Schiffman, C. K. Bensel, J. P. Obusek, and D. J. Gutekunst, "Effects of a lower-body exoskeleton device on metabolic cost and gait biomechanics during load carriage," *Ergonomics*, vol. 53, no. 10, pp. 1263–1275, 2010.

[13] K. Kong and D. Jeon, "Design and control of an exoskeleton for the elderly and patients," *IEEE/ASME Transactions on mechatronics*, vol. 11, no. 4, pp. 428–432, 2006.

[14] A. B. Zoss, H. Kazerooni, and A. Chu, "Biomechanical design of the berkeley lower extremity exoskeleton (bleex)," *IEEE/ASME Transactions on mechatronics*, vol. 11, no. 2, pp. 128–138, 2006.

[15] Y. Sankai, "Hal: Hybrid assistive limb based on cybernics," in *Robotics research*, pp. 25–34, Springer, 2010.

[16] K. A. Strausser and H. Kazerooni, "The development and testing of a human machine interface for a mobile medical exoskeleton," in *2011 IEEE/RSJ International Conference on Intelligent Robots and Systems*, pp. 4911–4916, IEEE, 2011.

[17] J. E. Pratt, B. T. Krupp, C. J. Morse, and S. H. Collins, "The roboknee: an exoskeleton for enhancing strength and endurance during walking," in *IEEE International Conference on Robotics and Automation, 2004. Proceedings. ICRA'04. 2004*, vol. 3, pp. 2430–2435, IEEE, 2004.

[18] S. Wang, L. Wang, C. Meijneke, E. Van Asseldonk, T. Hoellinger, G. Cheron, Y. Ivanenko, V. La Scaleia, F. Sylos-Labini, M. Molinari, *et al.*, "Design and control of the mindwalker exoskeleton," *IEEE transactions on neural systems and rehabilitation engineering*, vol. 23, no. 2, pp. 277–286, 2014.

[19] H.-g. Kim, S. Park, and C. Han, "Design of a novel knee joint for an exoskeleton with good energy efficiency for load-carrying augmentation," *Journal of Mechanical Science and Technology*, vol. 28, no. 11, pp. 4361–4367, 2014.

[20] H.-g. Kim, J.-w. Lee, J. Jang, S. Park, and C. Han, "Design of an exoskeleton with minimized energy consumption based on using elastic and dissipative elements," *International Journal of Control, Automation and Systems*, vol. 13, no. 2, pp. 463–474, 2015.

[21] T. Zhang and H. Huang, "A lower-back robotic exoskeleton: Industrial handling augmentation used to provide spinal support," *IEEE Robotics & Automation Magazine*, vol. 25, no. 2, pp. 95–106, 2018.

[22] J.-W. Lee and G. Kim, "Design and control of a lifting assist device for preventing lower back injuries in industrial athletes," *International Journal of Precision Engineering and Manufacturing*, vol. 20, no. 10, pp. 1825–1838, 2019.

[23] J. C. Perry, J. Rosen, and S. Burns, "Upper-limb powered exoskeleton design," *IEEE/ASME transactions on mechatronics*, vol. 12, no. 4, pp. 408–417, 2007.

[24] R. A. R. C. Gopura, K. Kiguchi, and Y. Li, "Sueful-7: A 7dof upper-limb exoskeleton robot with muscle-model-oriented emg-based control," in *2009 IEEE/RSJ International Conference on Intelligent Robots and Systems*, pp. 1126–1131, IEEE, 2009.

[25] A. Chiri, N. Vitiello, F. Giovacchini, S. Roccella, F. Vecchi, and M. C. Carrozza, "Mechatronic design and characterization of the index finger module of a hand exoskeleton for post-stroke rehabilitation," *IEEE/ASmE Transactions on mechatronics*, vol. 17, no. 5, pp. 884–894, 2011.

[26] A. Wege and G. Hommel, "Development and control of a hand exoskeleton for rehabilitation of hand injuries," in *2005 IEEE/RSJ International Conference on Intelligent Robots and Systems*, pp. 3046–3051, IEEE, 2005.

[27] M. B. Näf, K. Junius, M. Rossini, C. Rodriguez-Guerrero, B. Vanderborght, and D. Lefeber, "Misalignment compensation for full human-exoskeleton kinematic compatibility: state of the art and evaluation," *Applied Mechanics Reviews*, vol. 70, no. 5, 2018.

[28] R. Mallat, M. Khalil, G. Venture, V. Bonnet, and S. Mohammed, "Human-exoskeleton joint misalignment: a systematic review," in *2019 Fifth International Conference on Advances in Biomedical Engineering (ICABME)*, pp. 1–4, IEEE, 2019.

[29] H. In, B. B. Kang, M. Sin, and K.-J. Cho, "Exo-glove: A wearable robot for the hand with a soft tendon routing system," *IEEE Robotics & Automation Magazine*, vol. 22, no. 1, pp. 97–105, 2015.

[30] Z. Yao, C. Linnenberg, R. Weidner, and J. Wulfsberg, "Development of a soft power suit for lower back assistance," in *2019 International Conference on Robotics and Automation (ICRA)*, pp. 5103–5109, IEEE, 2019.

[31] C. T. O'Neill, N. S. Phipps, L. Cappello, S. Paganoni, and C. J. Walsh, "A soft wearable robot for the shoulder: Design, characterization, and preliminary testing," in *2017 International Conference on Rehabilitation Robotics (ICORR)*, pp. 1672–1678, IEEE, 2017.

[32] C. O'Neill, T. Proietti, K. Nuckols, M. E. Clarke, C. J. Hohimer, A. Cloutier, D. J. Lin, and C. J. Walsh, "Inflatable soft wearable robot for reducing therapist fatigue during upper extremity rehabilitation in severe stroke," *IEEE Robotics and Automation Letters*, vol. 5, no. 3, pp. 3899–3906, 2020.

[33] A. T. Asbeck, S. M. De Rossi, I. Galiana, Y. Ding, and C. J. Walsh, "Stronger, smarter, softer: next-generation wearable robots," *IEEE Robotics & Automation Magazine*, vol. 21, no. 4, pp. 22–33, 2014.

[34] Y. soo Kwak, "Hyundai Motor Group develops wearable robot." https://www.koreatimes.co.kr/www/tech/2019/09/693_275084.html, 2019. [Online; accessed 28-October-2021].

[35] L. HeroWear, "Women Lift Every Day." https://herowearexo.com/suited-for-all/, 2021. [Online; accessed 5-November-2021].

[36] N. Jarrassé, M. Tagliabue, J. V. Robertson, A. Maiza, V. Crocher, A. Roby-Brami, and G. Morel, "A methodology to quantify alterations in human upper limb movement during co-manipulation with an exoskeleton," *IEEE Transactions on neural systems and Rehabilitation Engineering*, vol. 18, no. 4, pp. 389–397, 2010.

[37] N. Jarrassé and G. Morel, "Connecting a human limb to an exoskeleton," *IEEE Transactions on Robotics*, vol. 28, no. 3, pp. 697–709, 2011.

[38] D. Zanotto, Y. Akiyama, P. Stegall, and S. K. Agrawal, "Knee joint misalignment in exoskeletons for the lower extremities: Effects on user's gait," *IEEE Transactions on Robotics*, vol. 31, no. 4, pp. 978–987, 2015.

[39] X. Yang, T.-H. Huang, H. Hu, S. Yu, S. Zhang, X. Zhou, A. Carriero, G. Yue, and H. Su, "Spine-inspired continuum soft exoskeleton for stoop lifting assistance," *IEEE Robotics and Automation Letters*, vol. 4, no. 4, pp. 4547–4554, 2019.

[40] D. A. Winter, *Biomechanics and motor control of human movement*. John Wiley & Sons, 2009.

[41] L. Zollo, B. Siciliano, C. Laschi, G. Teti, and P. Dario, "An experimental study on compliance control for a redundant personal robot arm," *Robotics and Autonomous systems*, vol. 44, no. 2, pp. 101–129, 2003.

[42] L. Zollo, B. Siciliano, A. De Luca, E. Guglielmelli, and P. Dario, "Compliance Control for an Anthropomorphic Robot with Elastic Joints: Theory and Experiments," *Journal of Dynamic Systems, Measurement, and Control*, vol. 127, no. 3, pp. 321–328, 2004.